

# Luminosity–Colours relations for thin disc main-sequence stars

S. Bilir,<sup>1\*</sup> S. Karaali<sup>2</sup>, S. Ak<sup>1</sup>, E. Yaz<sup>1</sup>, A. Cabrera-Lavers<sup>3,4</sup>, K. B. Coşkunoglu<sup>1</sup>

<sup>1</sup>*Istanbul University Science Faculty, Department of Astronomy and Space Sciences, 34119, University-Istanbul, Turkey*

<sup>2</sup>*Beykent University, Faculty of Science and Letters, Department of Mathematics and Computer, Ayazağa 34396, Istanbul, Turkey*

<sup>3</sup>*Instituto de Astrofísica de Canarias, E-38205 La Laguna, Tenerife, Spain*

<sup>4</sup>*GTC Project Office, E-38205 La Laguna, Tenerife, Spain*

Accepted 2008 month day. Received year month day;

## ABSTRACT

In this study we present the absolute magnitude calibrations of thin disc main-sequence stars in the optical ( $M_V$ ), and in the near-infrared ( $M_J$ ). Thin disc stars are identified by means of *Padova* isochrones, and absolute magnitudes for the sample are evaluated via the newly reduced *Hipparcos* data. The obtained calibrations cover a large range of spectral types: from A0 to M4 in the optical and from A0 to M0 in the near-infrared. Also, we discuss the effects of binary stars and evolved stars on the absolute magnitude calibrations. The usage of these calibrations can be extended to the estimation of galactic model parameters for the thin disc individually, in order to compare these parameters with the corresponding ones estimated by  $\chi^2_{min}$  statistics (which provides galactic model parameters for thin and thick discs, and halo simultaneously) to test any degeneracy between them. The calibrations can also be used in other astrophysical researches where distance plays an important role in that study.

**Key words:** Galaxy: disc, Galaxy: solar neighbourhood, stars: distances

## 1 INTRODUCTION

The distance of an astronomical object plays an important role in deriving intrinsic luminosities of stars, in calculating accurate masses for binary system components and in answering questions about galactic structure. Particularly, the distributions of three populations (i.e. thin and thick discs, and halo) in the Galaxy can be determined using the distances of the concerning stars. For nearby stars, the most appropriate procedure for distance determination is the trigonometric parallax. However, this procedure fails for distant stars due to large errors in their trigonometric parallaxes. In this case, photometric parallax replaces the trigonometric one. This alternative requires absolute magnitude determination which needs a lot of work, though not as much as the former one.

The photometric parallax can be evaluated in different ways. Many astronomers prefer an absolute magnitude-colour diagram for a star category. For example, Phleps et al. (2000) separated their star sample into two subsamples, disc and halo, according to their  $(r - i)$  colours and they used two absolute magnitude diagrams to evaluate their absolute magnitudes.

Karaali et al. (2003); Karaali, Bilir & Hamzaoglu (2004) and Bilir, Karaali & Gilmore (2006) separated their star samples into three populations, i.e. thin and thick discs, and halo, and they used the absolute magnitude-colour diagrams of three globular clusters with the same metallicity of the corresponding population. Bilir, Karaali & Tunçel (2005) calibrated the  $M_g$  absolute magnitudes of late type disc dwarfs with  $(g - r)$  and  $(r - i)$  colours in *SDSS* system. The works of Siegel et al. (2002) and Jurić et al. (2008) are examples for distance estimation based on photometric parallax. Another procedure for absolute magnitude determination is based on the use of colours and individual UV-excesses of stars relative to a standard absolute magnitude-colour diagram, such as Hyades (Laird, Carney & Latham 1988; Karaali et al. 2003; Karaali, Bilir & Tunçel 2005). In this procedure, one does not need to separate the stars into different population types. Additionally, individual UV-excess for each star results in more precise absolute magnitudes relative to the procedure where a single colour magnitude diagram is used for all stars in a population.

Despite the extensive applications of the aforementioned procedures in the previous paragraph, additional constraints can be considered for obtaining a more reliable one. We applied three limitations, i.e. age, metallicity and surface gravity, to a star sample and calibrate the absolute mag-

\* E-mail: sbilir@istanbul.edu.tr

nitude of thin disc stars as a function of two colours. All these data were provided from *Padova* database of stellar evolutionary tracks and isochrones (Marigo et al. 2008) by using a web interface<sup>1</sup>. For the thin disc stars we adopted a range of age of  $0 \leq t \leq 10$  Gyr, and the metal abundance is assumed to be  $0.01 \leq z \leq 0.03$  (solar metal abundance  $z_{\odot} = 0.019$ ), corresponding to the metallicity interval  $-0.30 \leq [M/H] \leq 0.20$  dex. Finally, evolved stars were excluded from the sample by imposing a third constraint, i.e. surface gravity  $\log g > 4$ . Thus, we should supply a homogeneous thin disc main-sequence sample by eliminating all thick disc and halo stars, as well as evolved (white dwarfs, sub-giants and giants) thin disc stars.

## 2 DATA AND REDUCTIONS

*BVI* photometric data and  $\pi$  parallaxes with relative errors  $(\sigma_{\pi}/\pi) \leq 0.05$  for 11644 stars were taken from the newly reduced *Hipparcos* data (van Leeuwen 2007), whereas the *2MASS* (Two Micron All Sky Survey) near-infrared photometric data for the same stars were extracted of the Point-Source Catalogue and Atlas (Cutri et al. 2003). The *2MASS* photometric system comprises Johnson's *J* ( $1.25 \mu\text{m}$ ) and *H* ( $1.65 \mu\text{m}$ ) bands with the addition of *K<sub>s</sub>* ( $2.17 \mu\text{m}$ ) band, which is bluer than Johnson's *K*-band (Skrutskie et al. 2006). The  $E(B-V)$  colour-excesses were individually evaluated for each sample star making use of the maps of Schlegel, Finkbeiner & Davis (1998), and this was reduced to a value corresponding to the distance of the star by means of the equations of Bahcall & Soneira (1980). The  $E(B-V)$  iso-colour excess contours within 100 pc of solar neighbourhood are given in Fig. 1. The distribution of  $E(B-V)$  for the star sample for two distance intervals,  $0 < d \leq 40$  pc and  $40 < d \leq 70$  pc, have a peak at  $E(B-V) = 0.0041$  and  $E(B-V) = 0.0098$  mag which are rather close to the ones of Holmberg, Nordström & Andersen (2007). Holmberg et al. (2007) evaluated the colour excesses,  $E(B-V) = 0.0034$  and  $E(B-V) = 0.0065$  mag, for the same distance intervals by using Strömgren photometry, respectively. The transformation of  $E(b-y)$  reddening to the  $E(B-V)$  one is carried out by the equation  $E(B-V) = 1.35 \times E(b-y)$ . The excellent agreement between both sets of reddening data confirms the reduction equations of Bahcall & Soneira (1980) and the accuracy of the colour-excesses used in our work.

Thus, colours and magnitudes from the sample stars are de-reddened by using the following two sets of equations, one for the *BVI* data (Eq. 1) and one for the *2MASS* (Eq. 2) photometry:

$$\begin{aligned} V_0 &= V - 3.1 \times E(B-V), \\ (B-V)_0 &= (B-V) - E(B-V), \\ (V-I)_0 &= (V-I) - 1.25 \times E(B-V). \end{aligned} \quad (1)$$

$$\begin{aligned} J_0 &= J - 0.887 \times E(B-V), \\ (J-H)_0 &= (J-H) - 0.322 \times E(B-V), \\ (H-K_s)_0 &= (H-K_s) - 0.182 \times E(B-V). \end{aligned} \quad (2)$$

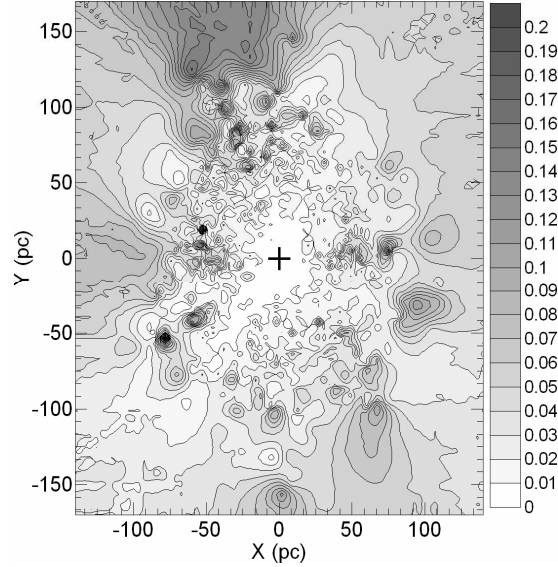


**Figure 1.** The  $E(B-V)$  iso-colour-excess contours within 100 pc of the solar neighbourhood. Here,  $X$  and  $Y$  are heliocentric galactic coordinates oriented towards the galactic centre and galactic rotation, respectively.

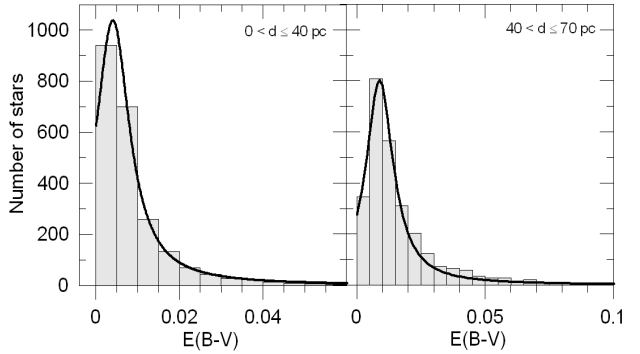


**Figure 2.** Distribution of the  $E(B-V)$  colour-excess for the star sample for two distance intervals  $0 < d \leq 40$  and  $40 < d \leq 70$  pc. The  $E(B-V)$  colour-excesses corresponding to these distributions are in good agreement with the ones of Holmberg et al. (2007).

(see also, Bilir, Güver & Aslan 2006; Ak et al. 2007).

The absolute magnitude of each star is evaluated by the combination of its de-reddened apparent magnitude and its distance estimated using its trigonometric parallax. The corresponding propagated errors were calculated as  $\sigma M = 2.17(\sigma_{\pi}/\pi) + \sigma m$ , where  $(\sigma_{\pi}/\pi)$  and  $\sigma m$  are the relative parallax error and the error of the apparent magnitude in the relevant photometric system, respectively.

## 3 THE PROCEDURE AND ABSOLUTE MAGNITUDE CALIBRATION

The procedure consists of the calibration of the absolute magnitudes for thin disc main-sequence stars with two colours: one sensitive to early-type (hot) and another sensitive to late-type (cool) stars, providing a large range of

<sup>1</sup> <http://stev.oapd.inaf.it/~lgirardi/cgi-bin/cmdr>

absolute magnitudes for the thin disc population. We calibrated  $M_V$  absolute magnitudes with  $(B - V)_0$  and  $(V - I)_0$ , for the *BVI* photometry and  $M_J$  absolute magnitudes with  $(J - H)_0$  and  $(H - K_s)_0$  for the *2MASS* data. As it was stated in Section 1, we limited the metallicity, the age, and the surface gravity with the following constraints:  $-0.30 \leq [M/H] \leq 0.20$  dex,  $0 \leq t \leq 10$  Gyr, and  $\log g > 4$ . By doing this we avoid any contamination due to thick disc and halo stars, as well as from evolved thin disc stars. Hence, our calibrations should provide precise absolute magnitudes for thin disc main-sequence stars.

### 3.1 Absolute magnitude calibration for *BVI* photometry

We applied a series of limitations in the absolute magnitude calibration for *BVI* photometry. First of all, we limited our star sample with absolute magnitudes  $0 < M_V < 12$ . This limitation reduced the original star sample from 11644 to 10654. Then, we applied the procedure described in Section 2 to the *Padova* isochrones with metallicity and age limitations mentioned above (Marigo et al. 2008) which separates the thin disc stars with different luminosity classes (dwarf and evolved stars) from the sample of 10654 stars. At the third step, we applied the constraint for being a main-sequence star, i.e.  $\log g > 4$ . Thus, the sample reduced to 6117 stars. Fig. 3 shows the colour-absolute magnitude diagram for the original sample (11644 stars) and the upper and lower envelopes of the final sample, i.e. thin disc main-sequence stars. Then we adopted the  $M_V$  calibration as follows and evaluated the coefficients by the least-squares method, for the final sample:

$$M_V = a_1(B - V)_0^2 + b_1(V - I)_0^2 + c_1(B - V)_0(V - I)_0 + d_1(B - V)_0 + e_1(V - I)_0 + f_1. \quad (3)$$

The numerical values of the coefficients and their errors, as well as the corresponding standard deviations and the squared correlation coefficients are all given in Table 1. The calibration described by Eq. 3 covers a large range of thin disc main-sequence stars, i.e.  $-0.15 < (B - V)_0 < 1.60$ ,  $-0.15 < (V - I)_0 < 2.90$ , and  $0 < M_V < 12$ , that corresponds to the spectral types A0-M4.

### 3.2 Absolute magnitude calibration for *2MASS* photometry

The procedure described in Section 2 and the limitations applied in Section 3.1 produced 4449 main-sequence stars with *2MASS* photometric data, 93 per cent of the best quality following the survey criteria (labeled in the catalogue as AAA). Here, the star sample is limited with absolute magnitude  $0 < M_J < 6$ . The  $M_J/(J - H)_0$  colour-magnitude diagram for all stars taken from newly reduced *Hipparcos* catalogue (11644 stars) and the upper and lower envelopes for the final sample, i.e. thin disc main-sequence stars, are given in Fig. 4. We adopted an absolute magnitude calibration for the *2MASS* data similar to the *BVI* ones as follows:

$$M_J = a_2(J - H)_0^2 + b_2(H - K_s)_0^2 + c_2(J - H)_0(H - K_s)_0 + d_2(J - H)_0 + e_2(H - K_s)_0 + f_2. \quad (4)$$

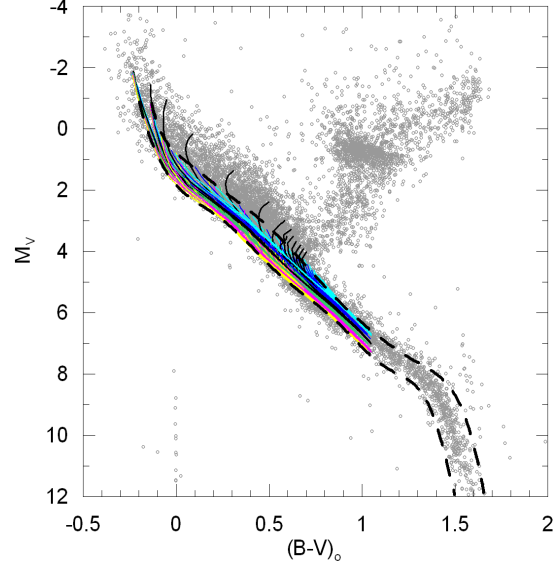


**Figure 3.**  $M_V/(B - V)_0$  colour-absolute magnitude diagram for the original sample. The upper and lower envelopes (the dashed lines) show the final sample, i.e. thin disc main-sequence stars. The thin curves correspond to *Padova* isochrones.

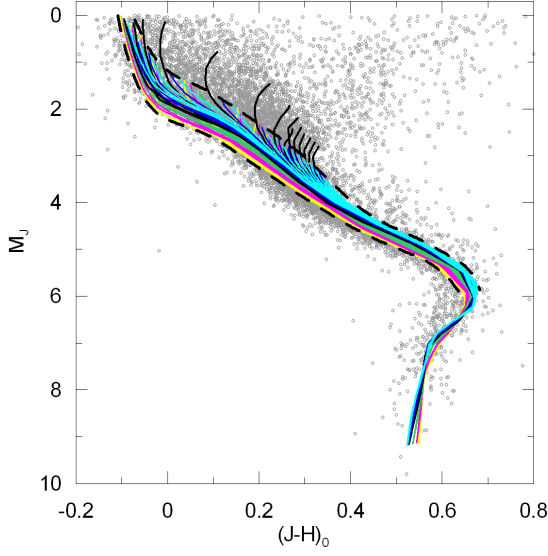
The numerical values of the coefficients and their errors, the corresponding standard deviations, and the squared correlation coefficients are given in Table 1. The calibration given in Eq. 4 covers a large range of thin disc main-sequence stars, as the one in Eq. 3, i.e.  $-0.16 < (J - H)_0 < 0.70$ ,  $-0.07 < (H - K_s)_0 < 0.26$ , and  $0 < M_J < 6$  corresponding to the spectral types A0-M0.

We plotted the errors of the observed colours against the intrinsic colours in Fig. 5 in order to test the accuracy of the observed colours. The lower uncertainties belong to  $(B - V)_0$  and  $(V - I)_0$  colours, whereas those for  $(J - H)_0$  and  $(H - K_s)_0$  are larger. The mean observational errors are about 0.01 ( $\sigma = \pm 0.02$ ) and 0.04 ( $\sigma = \pm 0.04$ ) mag in the optical and near-infrared colours, respectively. This is not surprising, because *2MASS* magnitudes were obtained from single-epoch observations, whereas optical magnitudes have been observed more than once. The mean errors introduce typically  $\pm 0.12$  and  $\pm 0.14$  mag uncertainties in  $M_V$  and  $M_J$ , respectively.

Unfortunately, random errors, presumably symmetric on the measured parallaxes, do not provide symmetric uncertainties on the computed distances. Therefore, a measured trigonometric parallax is very likely to be larger than the true parallax. The problem has already been noticed and studied by Lutz & Kelker (1973). Assuming a uniform space distribution of stars and a Gaussian distribution of observed parallaxes about a true parallax, Lutz & Kelker (1973) revealed that there is a systematic error in the computed distances which depends only upon the ratio  $(\sigma_\pi/\pi)$ , where  $\pi$  is the observed parallax. Jerzykiewicz (2001) showed that only the studies which are careful enough to use parallaxes with  $(\sigma_\pi/\pi) < 0.1$  could be excused as the bias would be negligible. This is the case in our work, where  $(\sigma_\pi/\pi) \leq 0.05$ . Actually, the Lutz-Kelker correction in absolute magnitude, taken from Lutz & Kelker (1973), is less than 0.03 mag. Hence, we omitted the mentioned bias in our study. Al-

**Table 1.** Coefficients and their standard errors for the Eqs. 3 ( $i=1$ ) and 4 ( $i=2$ ).  $R^2$  and  $s$  denotes the squared correlation coefficient and the standard deviation, respectively.

Eq.	$a_i$	$b_i$	$c_i$	$d_i$	$e_i$	$f_i$	$R^2$	$s$
3	-4.003 ( $\pm 0.532$ )	0.837 ( $\pm 0.192$ )	2.633 ( $\pm 0.671$ )	11.796 ( $\pm 0.359$ )	-5.691 ( $\pm 0.323$ )	1.122 ( $\pm 0.011$ )	0.98	0.27
4	-1.732 ( $\pm 0.109$ )	-7.734 ( $\pm 0.846$ )	1.084 ( $\pm 0.449$ )	7.509 ( $\pm 0.048$ )	2.208 ( $\pm 0.166$ )	1.305 ( $\pm 0.008$ )	0.98	0.19

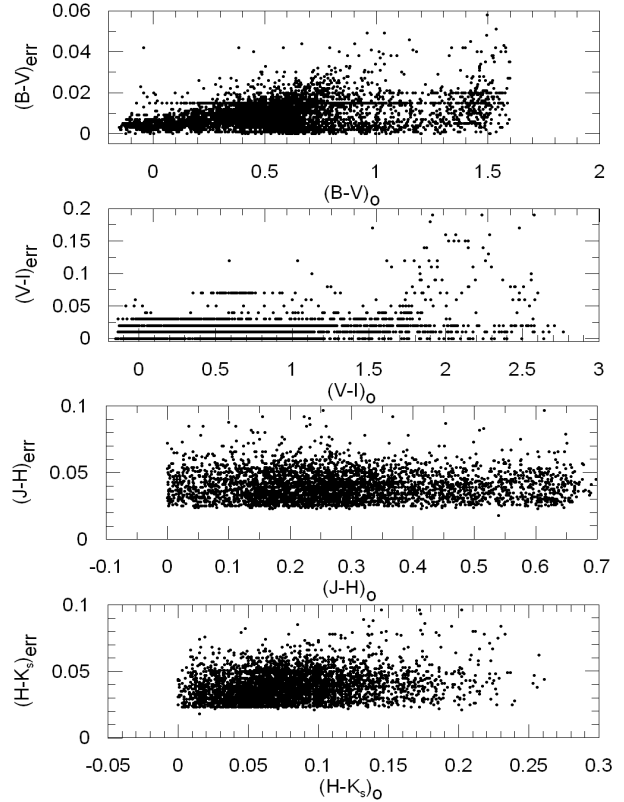
**Figure 4.**  $M_J/(J-H)_0$  colour-absolute magnitude diagram for the original sample. The upper and lower envelopes (the dashed lines) show the final sample, i.e. thin disc main-sequence stars. The thin curves correspond to *Padova* isochrones.

though no absolute magnitude calibration based on trigonometric parallaxes is present for the  $M_g$  absolute magnitude in *SDSS* system, one can use our recent transformation equations (Bilir et al. 2008).

### 3.3 Comparison of the estimated absolute magnitudes with the trigonometric parallaxes and synthetic photometry

We compared the absolute magnitudes estimated in this work with two sets of absolute magnitudes, one evaluated by means of the trigonometric parallaxes taken from the newly reduced *Hipparcos* catalogue (van Leeuwen 2007) and one taken from the stellar spectral flux library of Pickles (1998). Figs. 6 and 7 show the one-to-one correspondence of the absolute magnitudes  $M_{V_c}$  and  $M_{J_c}$ , respectively, estimated in this work and the corresponding ones evaluated from the newly reduced *Hipparcos* data, i.e.  $M_{V_{Hip}}$  and  $M_{J_{Hip}}$ .

Pickles (1998) offers the synthetic colours,  $M_{bol}$  bolometric absolute magnitudes and *BC* bolometric corrections for 131 stars with a large range of spectral type, O5-M6, and different luminosity-classes. The optical data are on the same scale of *UBVRI* photometry. Hence, it was easy to evaluate the  $M_{V_c}$  absolute magnitudes, by placing  $(B-V)_0$  and  $(V-I)_0$  colours into Eq. 3. However, the infrared colours and magnitudes scale differently than the *2MASS* data. Hence, we used the normalized equations of Carpenter (2001) to reduce Pickles' (1998) infrared data to *2MASS* colours and

**Figure 5.** Colour errors for the *BVI* and *2MASS* photometric data.

magnitudes. Then, we evaluated the  $M_{J_c}$  absolute magnitudes by placing the reduced  $(J-H)_0$  and  $(H-K_s)_0$  colours into Eq. 4. The original data of Pickles (1998) and the reduced ones according to normalized equations of Carpenter (2001) are given in Tables 2 and 3, respectively. Finally, we evaluated the  $M_{V_{Pic}}$  and  $M_{J_{Pic}}$  absolute magnitudes from the data in Table 3 and we compared them with the  $M_{V_c}$  and  $M_{J_c}$  absolute magnitudes, respectively (Figs. 8 and 9). There is a one-to-one correspondence in these figures as well. The slight declination at the faint end of absolute magnitudes in Fig. 9 is probably due to the different scales between the Pickles' (1998) and *2MASS*. We should add that the mentioned comparison has been carried out only for stars of solar metallicity.

## 4 DISCUSSION

We present two equations (Eqs. 3 and 4) derived from newly reduced *Hipparcos* data (van Leeuwen 2007) with the aim of applying these formulae to relatively distant stars whose distances are either newly reduced not accurately known or

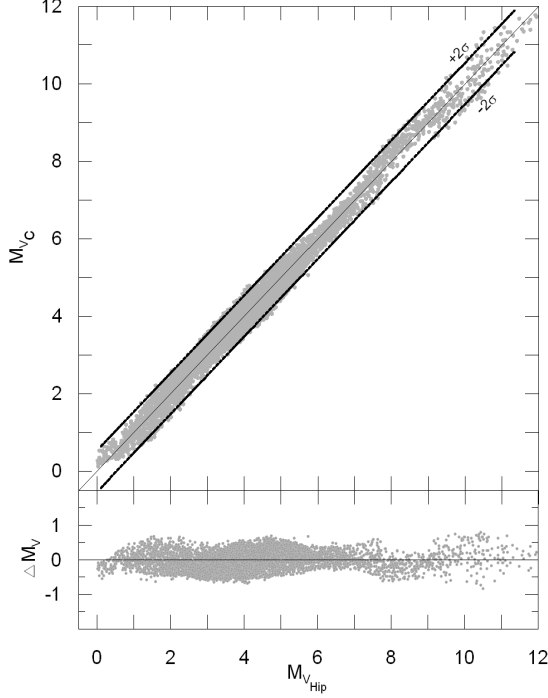


**Figure 6.** Absolute magnitudes, estimated by Eq. 3, versus optical absolute magnitudes calculated from newly reduced *Hipparcos* data (upper panel) and variation of the differences between two sets of absolute magnitudes (lower panel). All calibration stars in the figure are located in the prediction limit of  $2\sigma$ .

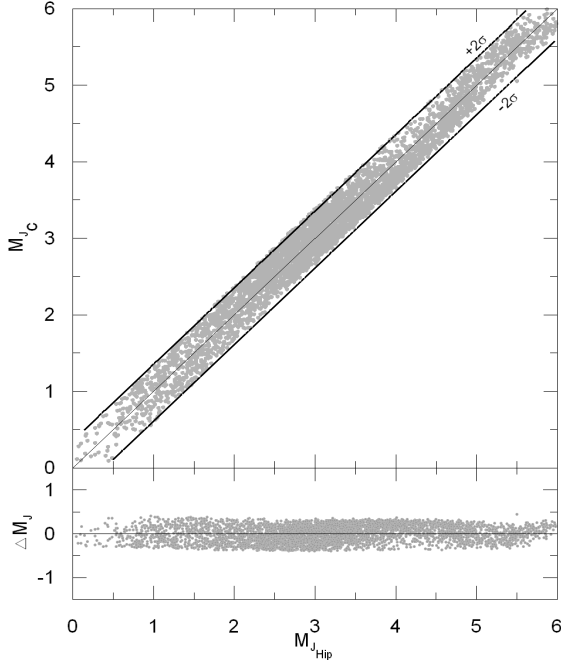


**Figure 7.** Absolute magnitudes, estimated by Eq. 4, versus near-infrared absolute magnitudes calculated from newly reduced *Hipparcos* data (upper panel) and variation of the differences between two sets of absolute magnitudes (lower panel). All calibration stars in the figure are located in the prediction limit of  $2\sigma$ .

**Table 2.** Original photometric data of Pickles (1998).

Sp. Type	$(B - V)$	$(V - I)$	$(R - I)$	$(J - H)$	$(H - K)$	$M_{V_{Pic}}$	$M_{K_{Pic}}$
A0V	0.015	0.011	0.023	0.000	0.000	0.48	0.49
A2V	0.029	0.049	0.043	0.010	0.010	1.18	1.32
A3V	0.089	0.102	0.065	0.030	0.020	1.33	1.45
A5V	0.153	0.156	0.103	0.060	0.020	1.69	1.33
A7V	0.202	0.241	0.131	0.090	0.030	2.09	1.62
F0V	0.303	0.378	0.203	0.130	0.030	2.98	2.30
F2V	0.395	0.457	0.246	0.170	0.040	3.27	2.63
F5V	0.458	0.496	0.255	0.230	0.040	3.50	2.44
F6V	0.469	0.562	0.292	0.260	0.050	3.83	2.70
F8V	0.542	0.615	0.312	0.300	0.040	4.04	2.79
G0V	0.571	0.671	0.351	0.350	0.050	4.24	2.94
G5V	0.686	0.735	0.372	0.340	0.070	4.78	3.27
K2V	0.924	0.968	0.448	0.500	0.090	6.19	3.96
K3V	0.930	1.109	0.513	0.540	0.100	6.80	4.40
K4V	1.085	1.232	0.570	0.580	0.110	7.21	4.56
K5V	1.205	1.361	0.610	0.610	0.110	7.64	4.77
K7V	1.368	1.578	0.750	0.660	0.150	8.21	5.11
M0V	1.321	1.709	0.847	0.670	0.170	8.62	4.94
M1V	1.375	1.874	0.993	0.660	0.280	9.05	5.16
M2V	1.436	2.020	1.061	0.660	0.200	9.58	5.44
M3V	1.515	2.436	1.362	0.640	0.230	10.63	5.96
M4V	1.594	2.781	1.565	0.620	0.270	11.54	6.24

**Table 3.** Data reduced by normalized equations of Carpenter (2001). The columns give: (1) Spectral type, (2)  $M_{V_{Pic}}$  absolute magnitude by Pickles (the same as in Table 2), (3)  $M_{V_c}$  absolute magnitude evaluated by Eq. 3, (4) and (5) and (6) reduced  $(J - H)$ ,  $(H - K_s)$  and  $M_J$  data (2MASS), and (7)  $M_{J_c}$  absolute magnitude evaluated by Eq. 4.

(1)	(2)	(3)	(4)	(5)	(6)	(7)
Sp. Type	$M_{V_{Pic}}$	$M_{V_c}$	$(J - H)$	$(H - K_s)$	$M_J$	$M_{J_c}$
A0V	0.48	1.24	-0.045	0.028	0.44	1.02
A2V	1.18	1.19	-0.035	0.038	1.28	1.11
A3V	1.33	1.59	-0.016	0.048	1.44	1.27
A5V	1.69	2.03	0.014	0.048	1.35	1.50
A7V	2.09	2.15	0.043	0.058	1.68	1.73
F0V	2.98	2.60	0.082	0.058	2.40	2.02
F2V	3.27	3.21	0.122	0.068	2.78	2.32
F5V	3.50	3.67	0.180	0.068	2.65	2.73
F6V	3.83	3.53	0.210	0.078	2.95	2.95
F8V	4.04	4.03	0.249	0.068	3.07	3.20
G0V	4.24	4.12	0.298	0.078	3.27	3.54
G5V	4.78	4.93	0.288	0.098	3.61	3.50
K2V	6.19	6.24	0.445	0.118	4.48	4.51
K3V	6.80	6.07	0.484	0.128	4.97	4.76
K4V	7.21	6.99	0.523	0.138	5.18	4.99
K5V	7.64	7.65	0.553	0.138	5.42	5.17
K7V	8.21	8.56	0.602	0.177	5.84	5.46
M0V	8.62	8.38	0.612	0.197	5.70	5.52
M1V	9.05	8.83	0.602	0.307	6.02	—
M2V	9.58	9.37	0.602	0.227	6.22	—
M3V	10.63	10.63	0.582	0.257	6.75	—
M4V	11.54	12.08	0.563	0.297	7.05	—

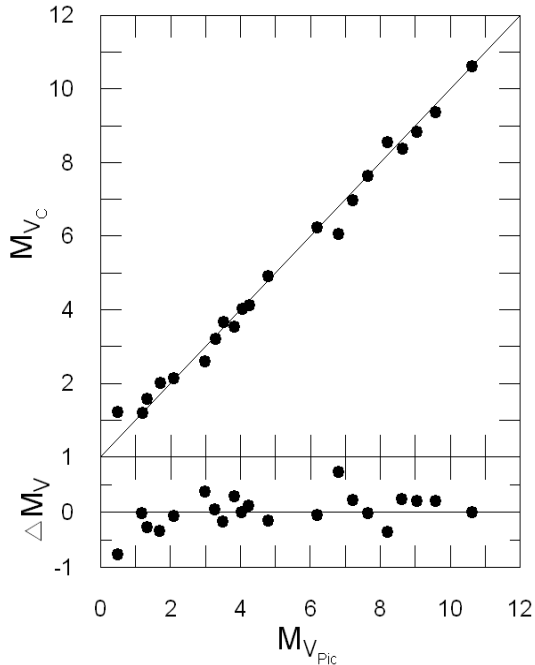


**Figure 8.** Absolute magnitudes, estimated by Eq. 3, versus optical absolute magnitudes calculated from Pickles’ data (upper panel) and variation of the differences between two sets of absolute magnitudes (lower panel).

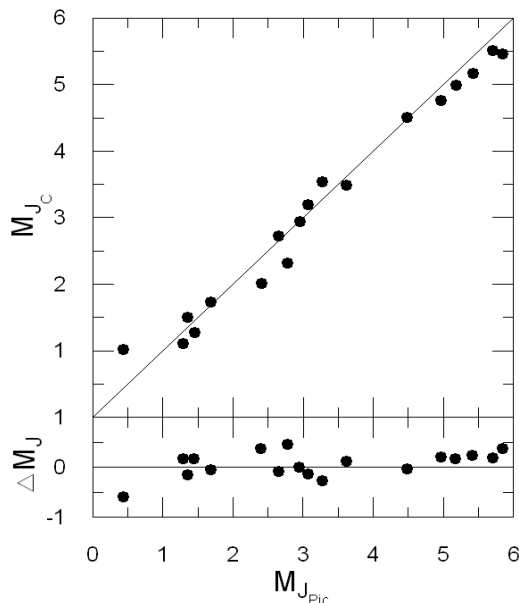


**Figure 9.** Absolute magnitudes, estimated by Eq. 4, versus near-infrared absolute magnitudes calculated from Pickles’ data (upper panel) and variation of the differences between two sets of absolute magnitudes (lower panel).

not known at all. To do this, one needs to obtain a sample of thin disc stars and replace the  $(B-V)_0$  and  $(V-I)_0$  colours with Eq. 3 or  $(J-H)_0$  and  $(H-K_s)_0$  colours with Eq. 4, depending on the preferred photometry. This procedure can supply the following contributions to the estimation of galactic model parameters:

- One can evaluate the space densities in the solar neighbourhood ( $r < 400$  pc – we assume all these stars belong to the thin disc) by using the *2MASS* data where the *SDSS* magnitudes are saturated; and combine them with space densities at larger distances evaluated by *SDSS* data. Thus, obtaining a continuous space density function from the Sun to large distances. This approach provides accurate galactic model parameters for the galactic components (thin and thick discs, and halo).
- This procedure provides individually estimated galactic model parameters for the thin disc. Hence, one can compare these parameters with the ones estimated by  $\chi^2_{min}$  statistics which provide galactic model parameters simultaneously for thin and thick discs, and halo; and we can test any possible degeneracy between different galactic model parameters. We should emphasize that the mentioned degeneracy is a serious problem for the galactic model parameters. Thus, we hope to contribute a little to this problem which is suffered by the galactic model researchers.

The absolute magnitude calibrations for the thin disc main-sequence stars with two colours, one sensitive to early type (hot) and another sensitive to late type (cool) stars, can also be used in other astrophysical researches, apart from the galactic model parameters estimation. Since absolute magnitude supplies the distance of a star, which plays an important role in the investigation of many properties of that star.

However, there are two significant issues which need to be considered on this subject, i.e. binary stars and evolved stars.

#### 4.1 Binary stars

A high fraction of stars are in fact binary systems and being a binary system makes stars appear brighter and redder than they normally are. Different fractional values (defined as  $f$ ) can be found in the literature. For example, using the data in the Gliese catalogue of nearby stars, Brosche (1964) found a value of  $f = 0.4$  for his simple model for the resolution criterion. On considering the local (within a distance of 10 pc) binary fraction, Reid (1991) concluded that the proportion of binaries among “stars” is consistent with a value ranging from 30 to 50 per cent. When all systems in question are binary stars, i.e.  $f = 1$ , Kroupa, Gilmore & Tout (1991) found that a single mass function provides the best representation of a single luminosity function. However, a smaller value can not be discarded with high confidence. Halbwachs (1986) used all available data on binary systems and concluded that the proportion of single stars among all stellar systems is at most 23 per cent when spectroscopic binaries are taken into account. An extensive long-term radial velocity study of the Hyades cluster reveals that at least 30 per cent of the cluster stars are spectroscopic binaries and that essentially all stars brighter than the Hyades main-sequence stars are in fact binary systems (Griffin et al. 1988).

The effect of binary stars were discussed in Kroupa, Tout & Gilmore (1990, 1993, hereafter KTG90 and KTG93, respectively) extensively as well as other effects such as metallicity, age, distance etc. KTG93 adopt the binary fraction  $f \sim 0.6 - 0.7$  as a reasonable value. They give the mentioned combined effects as “cosmic

**Table 4.** Scatter in absolute magnitude,  $\Delta M_V$  and  $\Delta M_J$ , as a function of binary fraction  $f$ .

$f$	$\Delta M_V$	$\Delta M_J$
0.0	0.000	0.000
0.1	0.057	0.044
0.2	0.102	0.077
0.3	0.136	0.101
0.4	0.172	0.124
0.5	0.208	0.148
0.6	0.248	0.171
0.7	0.294	0.196
0.8	0.348	0.226

scatter” as a function of  $(V - I)$  colour in the range  $0.5 < (V - I) < 4.5$ . These authors estimate the scatter belonging to binaries alone as  $\sigma = 0.27$  mag, if a fraction  $f = 0.8$  of all stars are unresolved binary systems. We adopted a simple but reasonable procedure, explained in the following paragraphs, to reveal the binarism effect in our work and to compare with the ones appeared in the studies cited above.

We separated the  $(B - V)_0$  and  $(J - H)_0$  colours into small bins and omitted a fraction of bright stars, each time, in these intervals. Then, we re-calibrated the absolute magnitudes  $M_V$  and  $M_J$  as a function of colours for the remaining stars. The fractions of binaries range from 0 to 80 per cent in steps of 10 per cent. Each time the locus of the stars on the colour-magnitude diagram moved to fainter absolute magnitudes. The mean of the differences between the absolute magnitudes estimated by the calibration in Section 3 and by these loci is adopted as the scatter due to the binaries in question (Table 4 and Fig. 10). Our procedure is based on the fact that binarism make stars too bright and too red. We calibrated the absolute magnitude scatter in  $f$ -absolute magnitude diagram,  $\Delta M_V$  and  $\Delta M_J$ , linearly (Fig. 11) as follows:

$$\Delta M_V = 0.411 \times f + 0.009, \quad (5)$$

$$\Delta M_J = 0.266 \times f + 0.014. \quad (6)$$

The last two equations can be used to reduce the estimated absolute magnitudes by an amount of scatter corresponding to the adopted fraction of binary stars. The scatter  $\sigma = 0.35$  mag in Table 4 is close to the one of KTG93, i.e.  $\sigma = 0.27$  mag, for the fraction  $f = 0.8$  of binary stars, confirming our simple but reasonable procedure used to reveal the fraction of binary stars and the linear regressions in Eqs. (5) and (6).

## 4.2 Evolved stars

A sample of field stars intrinsically brighter than an old star—with the same or similar spectral type—passed its turn-off is consisted of evolved stars, and they will be brighter and redder than a younger sample. In our case, the contamination of the evolved stars seems to be at a minimum due to the restrictions applied to the *Padova* isochrones in our work, i.e. the sample of the field stars are limited with metallicity  $-0.30 \leq [M/H] \leq 0.20$  dex, age  $0 \leq t \leq 10$  Gyr, and surface gravity  $\log g > 4$ . However, we applied the calibrations

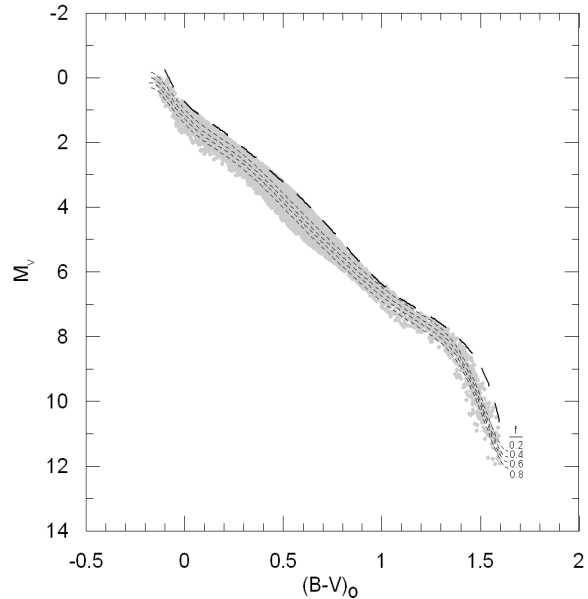


**Figure 10.** Lines indicating the fraction of binary stars in the  $M_V/(B - V)_0$  colour-magnitude diagram.

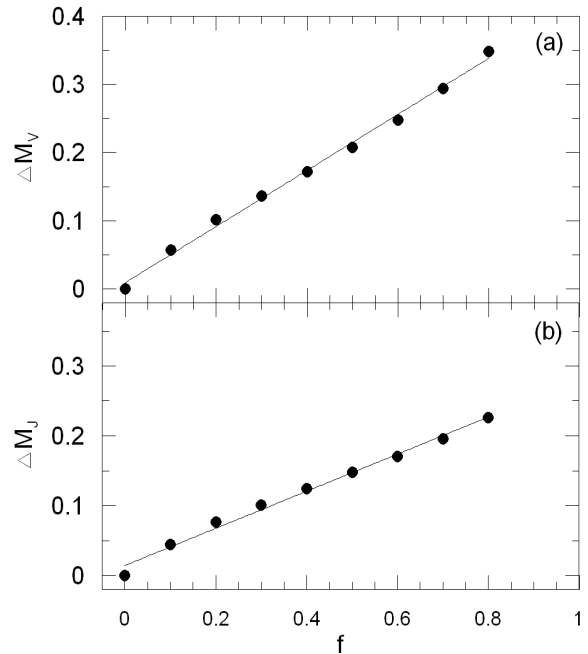


**Figure 11.** Scatter in absolute magnitude versus fraction of binary stars. (a)  $\Delta M_V \times f$  and (b)  $\Delta M_J \times f$ .

in Eqs. (3) and (4) to the stars of young cluster Hyades and compared the resulting absolute magnitudes with the ones estimated by the photometric parallaxes of the cluster stars. After a comprehensive study Perryman et al. (1998) stated that the Hyades cluster has 282 member stars. However, to increase the probability of the membership, we restricted the sample to 141 stars within 10 pc distance from the cluster center. It turned out that 81 of them were binary stars or variable stars (Mason et al. 1993; Patience et al. 1998, SIMBAD data center). Hence, the 60 Hyades stars used in our

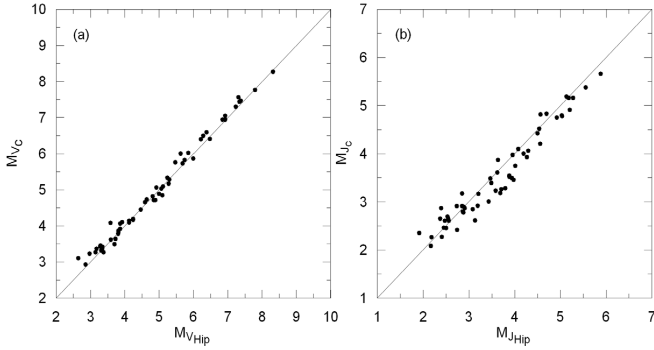


**Figure 12.** Absolute magnitudes, estimated via the calibrations presented in our work versus the ones evaluated by the parallaxes in the improved *Hipparcos* reduction. (a)  $M_{Vc} \times M_{VHip}$  and (b)  $M_{Jc} \times M_{JHip}$ .

work are single and non-variable stars within 10 pc from the center of Hyades cluster.

The absolute magnitudes of the Hyades sample estimated by Eqs. (3) and (4) are plotted against the ones calculated from their trigonometric parallaxes, taken from the newly reduced *Hipparcos* data (Fig. 12). There is an agreement between two sets of data, indicating that the field sample is not contaminated seriously by the evolved stars. The slight declination of the points towards the bright absolute magnitudes is due to single epoch observations of the *2MASS* data (Fig. 12b).

We should add that both binarism and evolution effects make the star brighter and redder, which means they both make the star move towards the same direction on the colour-magnitude diagram. Hence, the scatter in  $M_V$  and  $M_J$  absolute magnitudes cited in Eqs. (5) and (6) can be assumed as the combined effect of binarism and evolution. In this case, it is not surprising that the scatter  $\sigma = 0.35$  mag cited for the binary fraction  $f = 0.8$  is a bit larger than the one of KTG93, i.e.  $\sigma = 0.27$  mag, which corresponds to the binarism effect alone.

We wish to add that studying the effect of the evolved stars in the Hyades cluster revealed an unexpected issue for the cluster. Using the newly reduced *Hipparcos* data we derived a new distance modulus for the cluster:  $3.33 \pm 0.02$  mag. This value is slightly larger than the  $3.30 \pm 0.04$  mag of Perryman et al. (1998).

## 5 ACKNOWLEDGMENTS

We would like to thank the anonymous referee for his suggestion towards improving the manuscript. We acknowledge the use of the SIMBAD, database, the VizieR Catalogue Service operated at the CDS, and the use of the *2MASS* All-Sky Survey. One of us (S.K.) thanks to the Beykent University for financial support.

## REFERENCES

- Bilir S., Güver T., Aslan M., 2006, AN, 327, 693  
 Bilir S., Karaali S., Gilmore G., 2006, MNRAS, 366, 1295  
 Bilir S., Ak S., Karaali S., Cabrera-Lavers A., Chonis T. S., Gaskell C. M., 2008, MNRAS, 384, 1178  
 Brosche P., 1964, AN, 288, 33  
 Carpenter J. M., 2001, AJ, 121, 2851  
 Cutri R. M., et al., 2003, 2MASS All-Sky Catalog of Point Sources, CDS/ADC Electronic Catalogues, 2246  
 Griffin R. F., Griffin R. E. M., Gunn J. E., Zimmerman B. A., 1988, AJ, 96, 172  
 Halbwachs J. L., 1986, A&A, 168, 161  
 Holmberg J., Nordström B., Andersen J., 2007, A&A, 475, 519  
 Jerzykiewicz M., 2001, AcA, 51, 151  
 Jurić M., et al., 2008, ApJ, 673, 864  
 Karaali S., Bilir S., Karataş Y., Ak S. G., 2003, PASA, 20, 165  
 Karaali S., Bilir S., Hamzaoglu E., 2004, MNRAS, 355, 307  
 Karaali S., Bilir S., Tunçel S., 2005, PASA, 22, 24  
 Kroupa P., Tout C. A., Gilmore G., 1990, MNRAS, 244, 76  
 Kroupa P., Gilmore G., Tout C. A., 1991, MNRAS, 251, 293  
 Kroupa P., Tout C. A., Gilmore G., 1993, MNRAS, 262, 545  
 Laird J. B., Carney B. W., Latham D. W., 1988, AJ, 95, 1843  
 Lutz T. E., Kelker D. H., 1973, PASP, 85, 573  
 Marigo P., Girardi L., Bressan A., Groenewegen M. A. T., Silva L., Granato G. L., 2008, A&A, 482, 883  
 Mason B. D., McAlister H. A., Hartkopf W. I., Baguolo W. G. Jr., 1993, AJ, 105, 220  
 Patience J., Ghez A. M., Reid I. N., Weinberger A. J., Matthews K., 1998, AJ, 115, 1972  
 Perryman M. A. C., et al., 1998, A&A, 331, 81  
 Phleps S., Meisenheimer K., Fuchs B., Wolf C., 2000, A&A, 356, 108  
 Pickles A. J., 1998, PASP, 110, 863  
 Reid N., 1991, AJ, 102, 1428  
 Schlegel D. J., Finkbeiner D. P., Davis M., 1998, ApJ, 500, 525  
 Siegel M. H., Majewski S. R., Reid I. N., Thompson I. B., 2002, ApJ, 578, 151  
 Skrutskie M. F., et al., 2006, AJ, 131, 1163  
 van Leeuwen F., 2007, A&A, 474, 653